

A phenomenal behaviour of nanocrystalline NiFe_2O_4 : influence of secondary and parasitic phases on structure and magnetic property

A. Paul Blessington Selvadurai · V. Pazhanivelu · R. Murugaraj

Received: 7 July 2014 / Accepted: 22 December 2014 / Published online: 20 January 2015
© Springer-Verlag Berlin Heidelberg 2015

Abstract In this paper, we report the influence of secondary and parasitic magnetic phases on NiFe_2O_4 (NFO) nanoparticles synthesised during citrate gel method. Annealing at 773 K showed the presence of secondary and parasitic phases, whereas annealing at 1,073 K for 3 h showed the quenching of the secondary and parasitic phases. X-ray diffraction (XRD) analysis confirmed the nickel ferrite phase, with a trace amount of $\alpha\text{-Fe}_2\text{O}_3$ peak found and other phases being not traceable. The observed $\alpha\text{-Fe}_2\text{O}_3$ peak vanished at 1,073 K annealing, and a single phase of nickel ferrite was formed. The surface morphology of the samples was studied by SEM, which showed the fine grains of nickel ferrite. Raman spectra of the annealed samples were measured and analysed in the range of 1,000–100 cm^{-1} . Further analysis of isothermal M–H curve, zero-field-cooled and field-cooled (ZFC–FC) measurement and thermo-magnetisation M (T) measurements were performed with the aid of vibrating sample magnetometer on the prepared samples. The measured ZFC–FC curve showed an existence of spin-glass behaviour due to the parasitic phase for 773 K annealed sample, which is quite difficult to be identified using XRD and Raman spectra. Further, we also observed the room temperature coercivity $H_c = 430$ Oe from the M–H curve for the sample annealed at 773 K. Remarkably, both low-temperature and high-temperature M–T curve measurements showed the influence of secondary and parasitic phases for 773 and 1,073K annealed samples.

1 Introduction

Ferrites are prominent research interest materials for the past decades, exhibiting numerous technological applications, viz. high-density storage, magnetic fluid, telecommunication equipments, magnetically guided drug or radioactive nuclide delivery, and remote detoxification [1, 2]. Recently, it has been found that ferrites show magneto-electric (M-E) coupling by itself or induced through substitution [3, 4]. The observed M-E coupling is a potential opening for fabricating multifunctional devices [5]. Existing physical properties such as coercivity, magneto-crystalline anisotropy, magneto-strictive coefficient, chemical stability, mechanical hardness, electrical resistivity and Curie temperature (T_c) are found to be sensitive to their composition and microstructure, which depends on the processing conditions of ferrites.

Nickel ferrite (NiFe_2O_4) has an inverse spinel structure, in which Fe^{3+} ions are equally distributed in both A and B sites and Ni^{2+} ions in the B site. NiFe_2O_4 is most suitable for the aforementioned applications. Vast literature has been available for nanoparticles and bulk material [6–8]. In this study, citrate gel method was used to synthesise NiFe_2O_4 nanoparticles, which allows homogeneity and utilisation of less-expensive precursors. The attention on nanomaterials is due to their novel properties, especially in the nanoregime, e.g. the existence of superparamagnetic effect, a signature property of magnetic nanoparticles due to the size effect [9]. Tuning of properties either through multi-phase or by a single phase depends on the material applications, e.g. ferro/antiferrocomposites, and offers enhancement in magnetic properties such as coercivity and squareness ratio (SQ). Similarly, the minor additive inclusion increases the electrical properties, where they find their suitable applications in magnetic recording, switching devices and low loss

A. P. B. Selvadurai · V. Pazhanivelu · R. Murugaraj (✉)
Department of Physics, MIT Campus, Anna University,
Chennai 600044, India
e-mail: r.murugaraj@gmail.com

materials [10, 11]. Even, unintentionally formed secondary phases or impurities in ferrite system can mimic the above-said behaviours. Magnetic clusters, disorder interface due to non-magnetic impurity and antiferromagnetic phases formed naturally in the synthesis are reported [12, 13], exhibiting interesting properties when investigated.

In the present work, we show secondary and parasitic phases effect and its identification using magnetic measurement. The study is focussed to understand the effect of unintentionally formed secondary and parasitic magnetic phases in nano-crystalline nickel ferrite. Since the secondary and parasitic phases may have same structure with respect to the parent phase, it is difficult to identify their presence using X-ray diffractometer (XRD) and Raman spectra and these phases affect the magnetic properties of the parent phase. XRD shows only α -Fe₂O₃ presence, which coexists with NiFe₂O₄, but other phases could not be identified. Raman spectra also confirm the presence of α -Fe₂O₃ between the measured regions in 773 K annealed samples. Other phases from the Raman spectra are quite indistinguishable, due to the measured region of the spectra. With the aid of thermo-magnetisation M (T) measurements, we show the existence of the parasitic phase such as the presence of γ -Fe₂O₃ and NiO in the sample.

2 Experimental

Nano-crystalline nickel ferrite was synthesised using citrate combustion method. Ni (NO₃)₂·6H₂O and Fe (NO₃)₃·9H₂O of high purity were used as starter reagents for synthesis. The metal-to-citrate ratio was 1:3. The solution of nitrate and citrate was heated for several hours at 363 K, with a stirrer used for mixing. The solution was then kept in the muffle furnace at 573 K for 1 h. The resulting material after ignition had the appearance of a dark-brown ash, which was ground into fine powder and then annealed to 773 and 1,073 K for 3 h. XRD analysis of the powdered samples was performed using Bruker D2 phaser, a bench-top model using Cu-K_α radiation. Crystallite size of the 773 and 1,073 K annealed samples was measured using the Scherrer's equation.

$$D = \frac{0.9\lambda}{\beta_{1/2} \cos \theta} \text{ (nm)} \quad (1)$$

where λ is Cu-K_α and $\beta_{1/2}$ is the full-width at half-maximum. The Raman spectra are recorded in the range 100–1,000 cm⁻¹ using a confocal micro-Raman microscope (Renishaw inVia Reflex) with Ar⁺ ion laser source of 0.6 mW power and 514.5 nm excitation wavelength. The magnetic analysis was performed using vibrating sample magnetometer (VSM) Lakeshore-7410.

3 Results and discussion

3.1 XRD analysis

XRD patterns of NiFe₂O₄ for 773 and 1,073 K annealed samples are shown in Fig. 1. The XRD spectra of the samples were profile-fitted with the Fullprof program, with the space group of Fd-3 m. The calculated lattice parameter values are 8.307 and 8.345 Å for the annealed samples at 773 and 1,073 K, respectively. Numerous explanations for the increase in lattice constant in nanomaterials are available in the literature, such as change in oxygen coordination number, change in valence state of cations, crystallographic phase transformation and contribution of excess volume of grain boundary spins. [14–18]. Recently, it has been found that the lattice parameter for nickel ferrite shows a different trend on thermal annealing due to the Ph influence [19]. Probably these results suggest that surface modification is a reason behind it. In the present case, suppression of secondary and parasitic phases in the grain boundary surface due to annealing could have reduced the defect/vacancy in the structure, thereby increasing the lattice parameter.

The XRD spectra of the 773 K annealed sample through visual perception confirm that the nanocrystalline nickel ferrite with a slight impurity phase of α -Fe₂O₃ (*) is residing with the major NiFe₂O₄ phase as shown in Fig. 2. The usually formed secondary phases by the citrate method are α -Fe₂O₃, NiO and FeNi₃ [20]. Also, proton-incorporated γ -Fe₂O₃ phase with structural formula HFe₅O₈ in the as-synthesised powder of citrate precursor method is possible [21]. Thus, the citrate method offers a rare case of monophasic nickel ferrite, and hence, calcination at 1,000 °C for 1 h is required for the formation of pure nanocrystalline nickel ferrite or for any ferrite system [21].

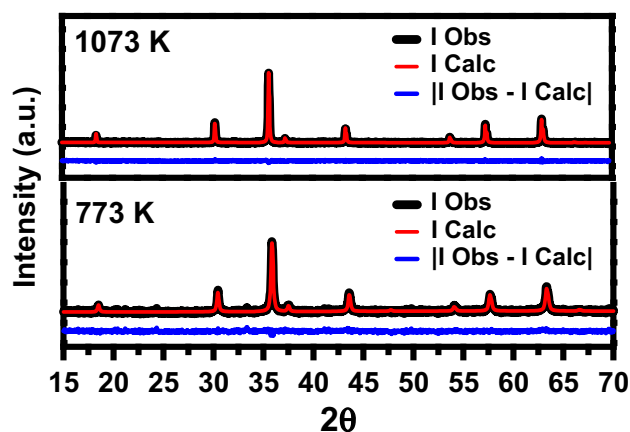


Fig. 1 Profile-fitted XRD pattern of nickel ferrite of 773 and 1,073 K annealed samples

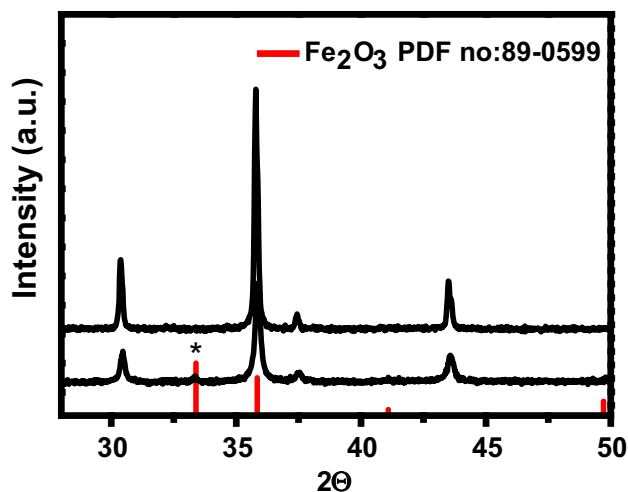


Fig. 2 α -Fe₂O₃ (*) and peak shift of nickel ferrite for 773 and 1,073 K annealed samples

The literature also shows that the formation of monophasic nickel ferrite is possible by sintering at 700 °C for 2 h [22]. Similarly, the 1,073 K annealed sample shows a single phase and, thus, conveys that above 700 °C, α -Fe₂O₃ and other phases are suppressed more effectively. But, interestingly, we note the presence of NiO and γ -Fe₂O₃ parasitic phases, from the (M–T) curve for the 773 and 1,073 K annealed samples. The γ -Fe₂O₃ phase appears for 773 K annealed sample, whereas it vanishes for 1,073 K annealed sample [23, 24]. XRD possesses limitation in identifying these parasitic phases, that is, if the quantity of the parasitic phase is smaller and also possesses a structure similar to the parent NiFe₂O₄, identifying such phases is difficult. Also, α -Fe₂O₃ is supposed to be formed from γ -Fe₂O₃, since γ -Fe₂O₃ is a meta-stable phase formed during synthesis [24]. Further, NiO also occurs as a secondary and parasitic phases naturally, to attain charge neutrality. We discuss briefly its presence and its influence, in the magnetic analysis section. The measured crystallite size shows a usual increasing trend on annealing, i.e. 30 and 76 nm for 773 and 1,073 K annealed samples, respectively.

3.2 SEM analysis

To confirm the morphology of the annealed sample, the SEM picture of 773 K annealed sample is shown in Fig. 3. From Fig. 3, it is observed that fine particles of irregular shapes were seen. The sizes of the particles are in close proximity to the measured values of crystallite size from the XRD spectra. SEM picture defies the shape anisotropy as the origin of high coercive field for the 773 K annealed sample observed in the M–H curve of Fig. 6. Such high coercive field occurs due to the shape anisotropy, particularly in the nanorods [25]. SEM image of 1,073 K annealed

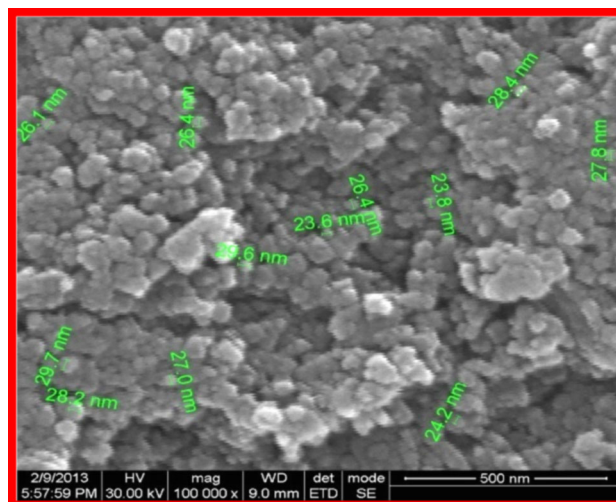


Fig. 3 SEM picture of 773 K annealed nickel ferrite

sample shows an irregular grain well grown due to thermal annealing, shown in Fig. 4.

3.3 Raman spectra analysis

Raman spectra of the annealed samples at 773 and 1,073 K are shown in Fig. 5. The spectra are measured between 1,000 to 100 cm⁻¹. Raman modes of A_{1g} + E_g + 3T_g are the characteristic of the cubic spinel (Fd-3 m) space group, which appears in the measured region [15]. From Fig. 5, the observed peaks at 704, 668, 570, 487, 460, 336 and 211 cm⁻¹ are very well consistent with the reported values of a nanocrystalline powder and single crystal samples [15, 26–29]. The increased relative intensity of the Raman

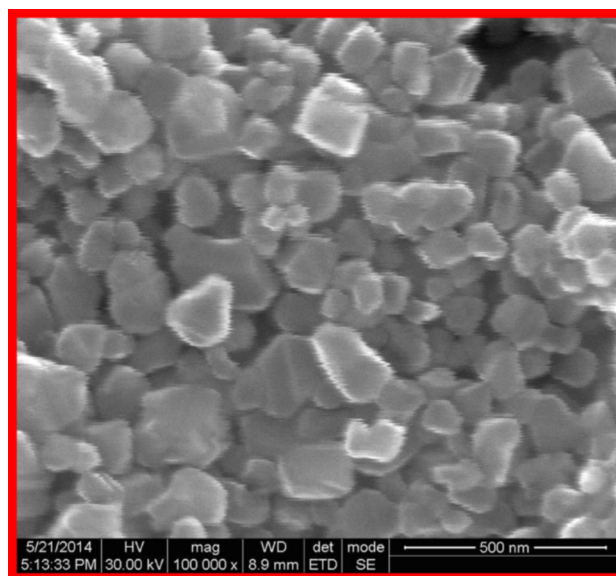


Fig. 4 SEM picture of 1,073 K annealed nickel ferrite

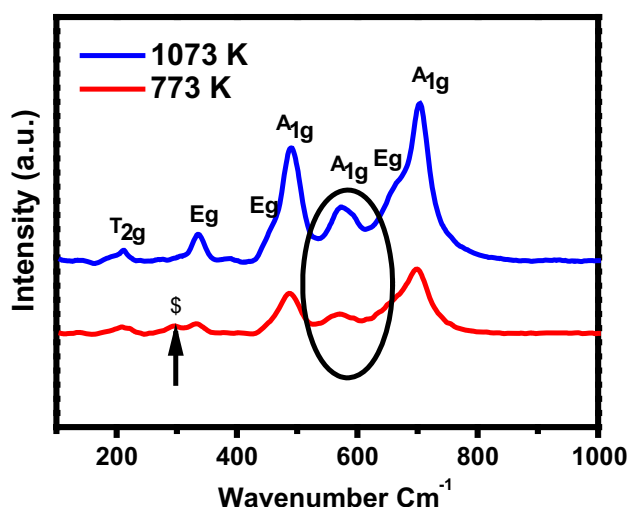


Fig. 5 Raman spectra of 773 and 1,073 K annealed nickel ferrite samples, \$ indicates α -Fe₂O₃ presence

spectra is attributed to an increase in crystallite size, which depends on the increase in annealing temperature, due to the growth of crystallite size [26]. Analysis of Raman spectra of the solid samples provides the optical modes of the parent compound, and they also provide information on the parasitic phase formed along with the parent compound [26, 28, 29]. However, the secondary phases of γ -Fe₂O₃ and Fe₃O₄ are quite difficult to identify both in Raman and in XRD analysis. Formation of Fe₃O₄ by the citrate method is quite impossible due to the method of synthesis. However, γ -Fe₂O₃ is formed by the citrate method usually [21]. γ -Fe₂O₃ has a similar mode of vibration and peak position compared to the parent compound, making it difficult to assign. Also, the present Raman spectra were measured only in 1000 cm⁻¹–100 cm⁻¹, which focuses on the parent modes of NFO compound alone.

Without the characteristic peak at 1,370 and 1,580 cm⁻¹, identifying γ -Fe₂O₃ is difficult in the measured region, and also overlapping of second-order overtone of A_{1g} and T_{2g} makes identifying γ -Fe₂O₃ difficult [28, 29]. The ellipse outline shown in Fig. 5 has a wide broadened peak at 550 cm⁻¹ for 773 K annealed sample, which corresponds to the stretching vibration of FeO₆ octahedral. The vibration band at 550 cm⁻¹ and 610–710 cm⁻¹ is assigned as A_{1g} phonon modes. The vibration band at 670–710 cm⁻¹ is a common feature of Raman spectrum that corresponds to inverse spinel stretching vibration of FeO₄ tetrahedral. However, the 1,073 K annealed sample shows that the vibration modes get strengthened and the disorder in the modes, particularly of 550 cm⁻¹ outline with an ellipse, gets suppressed [26]. The E_g and T_{2g} modes correspond to the symmetric and antisymmetric bending of oxygen atoms in Fe/Ni–O bond

at octahedral voids [19]. The arrow shown in Fig. 5 denoted as (\$) at 298 cm⁻¹ in 773 K annealed sample corresponds to α -Fe₂O₃ as reported [30], which does not match to any other peaks of nickel ferrite reported. It is also seen that this peak disappears on 1,073 K annealing. Thus, Raman spectra were in conjunction with the XRD results, where the iron oxide disappears on the increase in annealing temperature. Identifying the impurity phase of NiO is difficult, since it has a cubic symmetric with $K = 0$ offering no sign on the first-order Raman spectra. Also, Raman signal observed due to symmetric violation for NiO overlaps with the nickel ferrite in the measured region [31]. Thus, it is difficult to identify their phase from the Raman spectra.

3.4 Magnetic analysis

Figures 6 and 7 show an isothermal M–H curve of NFO samples, annealed at 773 and 1,073 K, respectively. The M–H behaviour was recorded at three different temperatures, viz. 20, 150 and 300 K. The saturation magnetisation Ms for the sample annealed at 773 K is 19.27 emu/g for 1.5 T at 300 K. On the other hand, it has an abrupt increase in Ms at 150 K and a slight increase at 20 K has also been observed. The M–H measurement for 1,073 K annealed sample shows a higher Ms value compared to 773 K annealed sample. A significant increase in Ms values at 150 and 20 K compared to Ms at 300 K is observed. For clear understanding, the relative change of magnetisation is depicted in Fig. 8, to discuss briefly. In the present case, the bulk magnetisation for NFO is 55 emu/g, which was a 100 % Ms value as given in the literature [19]. Both 773 and 1,073 K annealed samples have a smaller Ms value at 300 K. Since, the measured magnetisation of prepared

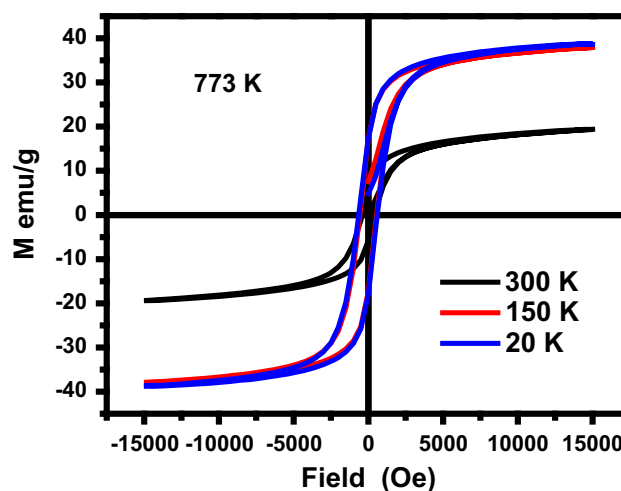


Fig. 6 Isothermal magnetisation M–H curve of nickel ferrite (annealed at 773 K)

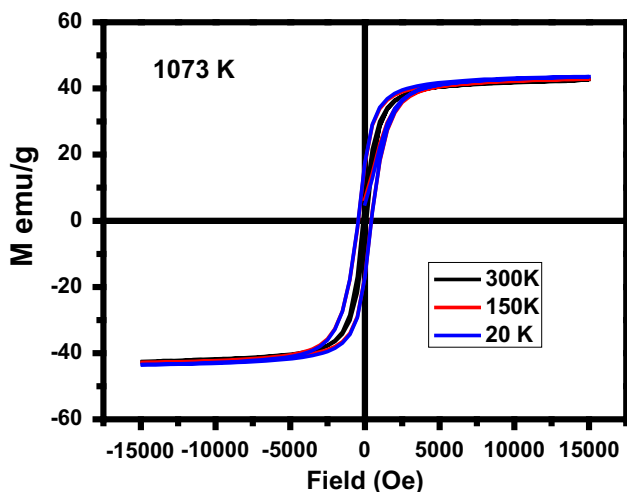


Fig. 7 Isothermal magnetisation M–H curve of nickel ferrite (annealed at 1,073 K)

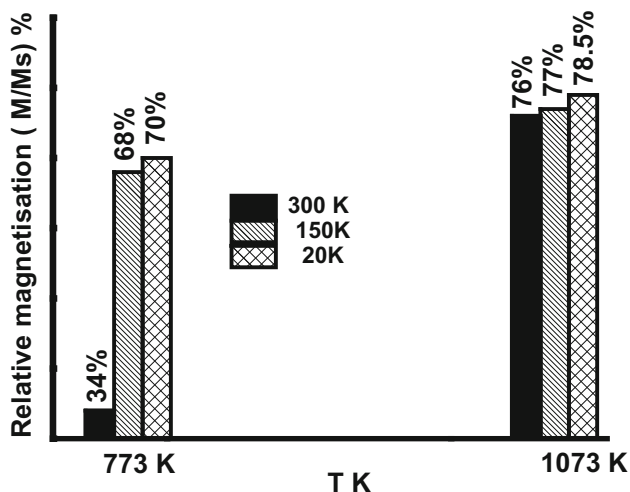


Fig. 8 Relative change in magnetisation for 773 and 1,073 K annealed nickel ferrite samples

ferrite depends on magnetic sublattices, crystallite size, and spin canting and antisite effect [32]. When the crystallite size decreases, it reduces the magnetisation value due to the canted spin acting as a passive layer on the surface of magnetic nanoparticles ascribed to the surface spin disorder [33]. In the present case, the measured magnetisation for 773 K annealed sample at 300 K is 34 % of the bulk value; at 150 K, it increases to 68 % and rises to 70 % of the bulk value at 20 K. This behaviour clearly indicates the existence of passive layer or surface disorder. Further, it is observed that only 2 % increment in magnetisation is observed between 150 and 20 K. The magnetisation in low temperature is suppressed possibly due to the existence of surface disorder or due to secondary and parasitic antiferromagnetism (AFM) phases. These results are certain by the thermo-magnetisation M (T) measurements, and it

suggests that the AFM might be the possible reason. Also, in accordance with the report [22], only 6 % change in Ms is observed between 300 and 5 K for 700 °C annealed sample. The Curie curve resembles more like our M–T curve, and the Curie temperature T_c is observed at 900 K. This result concludes that the 700 °C annealing process suppresses the parasitic phase, but not completely. However, the 1,073 K annealed sample shows a relatively high magnitude of magnetisation due to grain growth. It is interesting to note that the change in Ms measured between 300, 150 and 20 K is only 1 %. The observed Ms at 20 K shows 70 % for 773 K annealed in comparison with 1,073 K annealed, and it shows just 6 % of increase in the Ms at 300 K. This 6 % change is undoubtedly due to the grain growth and simultaneous suppression of secondary and parasitic phases. But, the increase in coercivity for 1,073 K annealed sample suggests that still FM–AFM interaction exists in it [34]. In addition, considering the secondary and parasitic phases, the NFO core also must be highly inverted because of the cation distribution [35].

The coercivity H_c of 773 K annealed sample records high coercivity of 470 Oe, and for 1,073 K annealed sample, it drastically reduces to 114 Oe. However, the coercivity at the low temperature increases drastically as shown in Fig. 9. In the literature, such high coercivity of 470 Oe and above is observed for the rod shape morphology, polycrystalline powder and in the polycrystalline thin film of nickel ferrite [25, 32, 36]. Generally, the coercivity is influenced by many factors such as magneto-crystallinity, microstrain, magnetic particle morphology, size distribution, anisotropy and magnetic domain size [37]. Therefore,

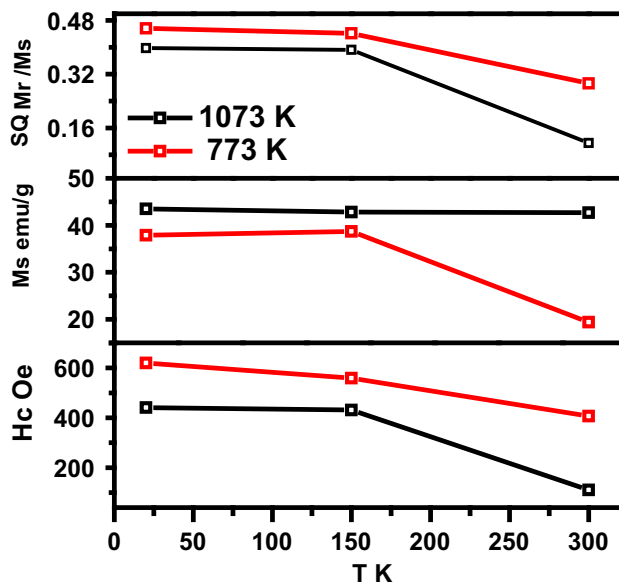


Fig. 9 Magnetisation parameters of nickel ferrite. (annealed at 773 and 1,073 K)

the observed high coercivity at 300 K could be due to the existence of the AFM that pins the domain wall in the ferrite for 773 K annealed sample, since the crystallite and grain size measured from XRD and SEM both show that the particle size is in the limit of single domain. Hence, the anisotropy of the single domain is greater and the presence of AFM phase could pin the domain movement more strongly for the increase in the coercivity in the 773 K annealed sample. On the other hand, the Neel temperature of the parasitic phases NiO and α -Fe₂O₃ was observed to be closer and greater than room temperature. Thus, the coercivity in isothermal curve shows increase in coercivity, similar to FM–AFM phase measured below Neel temperature [10, 34, 36]. The 1,073 K annealed sample has a coercivity of 114 Oe at 300 K. This decrease in coercivity is due to the grain growth and formation of domain walls, which reduces the magnetostatic energy due to the single domain and AFM phases and thus reduces the AFM pinning centres. The squareness (SQ) ratio M_r/M_s at 20 K for 773 K annealed sample is 0.45, a close proximity to a single domain value, that is, 0.5, and for 1,073 K annealed sample, it is 0.39, which shows the particle ranges from a single domain to multi-domain in nature and annealing increases the multi-domain behaviour in the sample [38]. The SQ value at 300 K for 773 and 1,073 K annealed samples shows a drastic change from 0.3 to 0.11. 0.3 SQ is higher to nickel ferrite at room temperature synthesis sample, and 0.1 SQ is the usually observed value [19].

The FC–ZFC curve is shown in Fig. 10. These measurements were in support to the measured M–H curve, which was taken at the applied field of $H_{app} = 500$ Oe. FC–ZFC curve shows the existence of irreversibility for both the samples. In the literature, this type of irreversibility occurs in superparamagnetic, spin-glass behaviour and interparticle interactions [33, 39, 40]. These

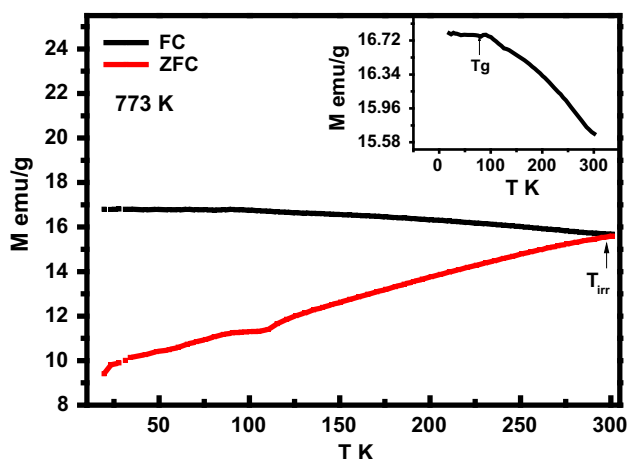


Fig. 10 ZFC–FC curve of nickel ferrite for 773 K annealed. *Inset* shows a FC curve indicating a surface spin-glass freezing (T_G)

phenomena should show a blocking temperature T_B . In the present case, no sign of T_B is observed from the measured FC–ZFC for both the samples. From Fig. 10, the FC curve shows that the decrease in temperature shows increases in measured magnetisation value for both annealed samples; in comparison, the abrupt rise of an FC curve is noted for 1,073 K annealed sample. This could be due to the response of magnetic domains, where the applied field switches the domain and domain walls, which moves easily for the annealed sample of 1,073 K, but an interesting behaviour is observed in ZFC curve, will be discussed later. The 773 K exhibits almost single domain particles, which is pinned effectively with AFM, the so-called secondary and parasitic phases. In this manner, the domain movements are hindered greatly, showing only a significant rise of M_s in the applied field. In Fig. 10, the inset of FC curve shows an interesting behaviour, that is, a decrease in magnetisation below ~ 100 K for 773 K annealed sample, such behaviour arises due to the interparticle and surface spin-glass freezing [41]. For the 1,073 K annealed sample, no such behaviour is identified in FC curve as shown in the inset of Fig. 11. The ZFC curve for both the annealed samples shows a steep fall of magnetisation on decreasing of temperature; this behaviour is due to the increase in coercivity or the increase in anisotropy energy. The steepness of fall is greater in the case of 773 K annealed sample than the 1,073 K annealed sample, and this observation in ZFC–FC curve is due to the strong pinning of FM/AFM interaction [42]. A closer view on the ZFC–FC of 1,073 K annealed sample shows an interesting behaviour, that is, different slopes of fall, which are represented as T_x and T_y , shown in Fig. 11 as inset 2. Since the ZFC curve usually represents the anisotropy/barriers in the sample, the T_x and T_y suggest different anisotropies/barriers present

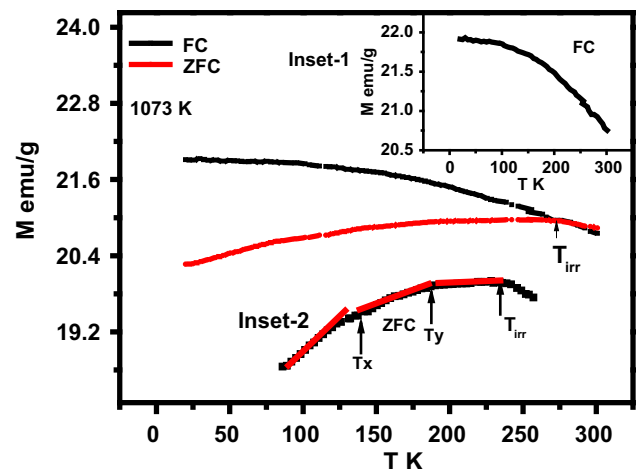


Fig. 11 ZFC–FC curve of nickel ferrite for 1,073 K annealed. *Inset 1* shows FC curve, and *Inset 2* shows the changes in ZFC curve

and it is due to the presence of AFM, which could be due to the uneven pinning or cluster-type pinning of AFM within the FM grains.

From the ZFC curve the pinning of FM/AFM in 773 and 1,073 K annealed samples was different, viz., a single domain to multiple domain could cause an AFM phase mixed into FM phase. Similar ZFC–FC curve is observed in the case of Dy-doped cobalt ferrite reported [34]. Therefore, we conclude that an inter-pinning of AFM/FM might be the possible reason, because our $M(T)$ curve for 1,073 K suggests the presence of AFM phase, which is discussed below. The difference in the $M_{FC}-M_{ZFC}$ curve shows their magnitude of separation in Fig. 12. For 773 K annealed sample, a greater separation confirms the stronger domain pinning effect. The temperature T_{irr} and ZFC curve is broadened for 1,073 K annealed samples, compared to 773 K annealed, and a decrease in magnetic anisotropy or weakening of dipole interactions reduces the T_{irr} [33]. This is due to the suppression of secondary and parasitic phases and grain growth. In addition to the above, a cusp is seen in the $M_{FC}-M_{ZFC}$ (shown in Fig. 12) for 773 K annealed sample and it disappears for 1,073 K annealed sample. This observed cusp could be due to the secondary and parasitic phases present in the sample, which is possibly the contribution of γ -Fe₂O₃, since this phase disappears in $M(T)$ curve for 1,073 K annealed as seen from the Fig. 13.

Thermo-magnetisation was measured by an applied field of 100 Oe is shown in Fig. 13 for both the annealed samples. The T_c of the prepared ferrite system is measured by taking the derivate of the $M(T)$ and is shown in the inset of Fig. 13. The measured T_c strongly depends on the cation distribution of the investigated ferrites family. The strength of the interaction is a function of the number of Fe³⁺–O–Fe³⁺ linkages present in tetrahedral (A) and octahedral [B]. In NiFe₂O₄, the exchange interaction is stronger for Fe³⁺ in

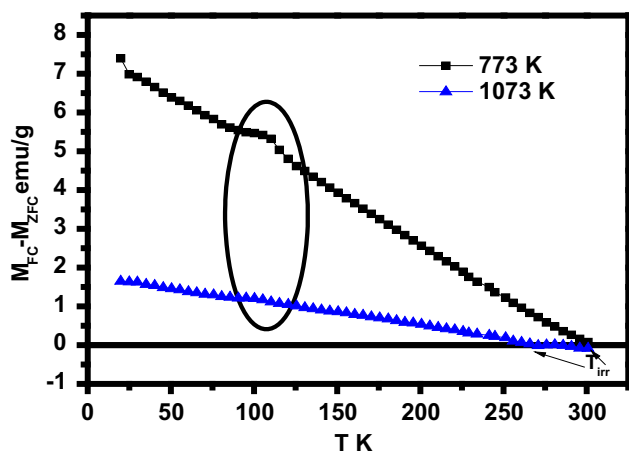


Fig. 12 $M_{FC}-M_{ZFC}$ curve of nickel ferrite (annealed at 773 and 1,073 K)

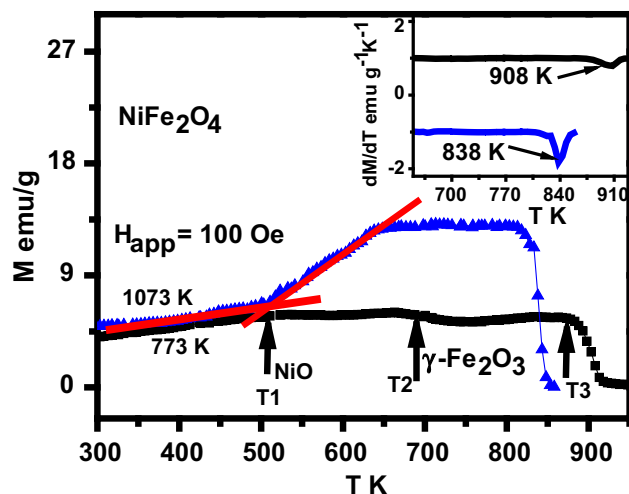


Fig. 13 Thermo-magnetisation of nickel ferrite for 773 and 1,073 K annealed. *Inset* shows Curie peaks for the sample

tetrahedral and octahedral sites, than the presence of Fe³⁺ ion and Ni²⁺/Fe²⁺ in A-A and B-B sites [43]. Therefore, the excess presence of Fe³⁺–O–Fe³⁺ linkage should increase the Curie temperature. The T_c of the bulk sample is 858 K [43]. But, the measured T_c of 773 K annealed sample is 908 K, and this enhancement in T_c is due to the presence of strong pinning of AFM with FM; the broader transition of the Curie peaks shows the nature of the crystallite size and the disorder of linkage. The Curie curve for 1,073 K annealed sample is almost similar to the reported value [43] and also close to the bulk NFO value. The decrease in Curie transition is possibly due to the increased linkage of Ni²⁺/Fe³⁺.

From Fig. 13, the $M(T)$ curve shows different transitions present in it and indicated as T1, T2 and T3 in the graph. The observed point T1 (i.e. 509 K), where the magnetisation flattens by changing the slope for 773 K annealed sample and rises drastically in the case of 1,073 K annealed sample. This change in magnetisation with temperature for a constant applied field literally means that the trapped magnetisation is released, i.e. pinned domain gets thermally activated. However, this behaviour is entirely different from the Hopkinson effect as hikes are observed near to the Curie point [44]. The 1,073 K annealed sample should change this T1 transition, as observed in the 773 K annealed sample. From the result, we suggest that this transition point may be due to the AFM phase present in the sample, and this temperature T1 matches well with the NiO bulk Neel transition temperature T_N [45]. Thus, NiO is formed in a citrate preparation method, which is not detectable from the XRD and Raman spectral analyses. The transition position T2 (669 K) is not observed for 1,073 K annealed sample, whereas T2 is observed only in the 773 K annealed sample. At T2, the magnetisation drops

significantly for 773 K annealed sample, which indicates the transition of γ -Fe₂O₃ to α -Fe₂O₃ [46]. The transition point T3 (872 K) indicates that it is a transition from ferromagnetic (FM)–paramagnetic (PM) for 773 K annealed sample. For the 1,073 K annealed sample, the M (T) measurement shows the NiO is not suppressed, i.e. at T1, the magnetisation raises and remains same, indicating that the pinned domains are saturated to the applied field. Also, there is no trace of γ -Fe₂O₃ phase present. Further, increase in temperature shows a transition of FM–PM. Thus, we confirm that secondary and parasitic phases are present in both the samples annealed at 773 and 1,073 K.

4 Conclusion

NiFe₂O₄ was prepared by citrate method and annealed at 773 and 1,073 K, respectively. The formation of NiFe₂O₄ phase was confirmed by XRD, SEM and Raman analyses. The XRD and Raman analysis show only the presence of impurity phase (α -Fe₂O₃) for 773 K annealed sample, and no other impurity phases were identified from the XRD and Raman analyses. The M–H curve measurement for 773 and 1,073 K annealed sample shows an increased coercivity for the measured temperature range. The high coercivity observed at 773 K annealed sample is due to the pinning of AFM phases present in the sample. The grain growth reduces the nature of pinning process as observed from M–H curve for 1,073 K annealed sample. Further, the FC–ZFC curve clearly shows such behaviour; stronger pinning in 773 K annealed sample is reduced; and local cluster-type pinning is observed in the ZFC of 1,073 K annealed sample. In addition to the above, we also observed a spin-glass freezing possibly due to secondary phase present in the samples. Temperature-dependent magnetisation M (T) measurement confirms and identifies the secondary and parasitic phases present in the 773 and 1,073 K annealed samples.

References

1. M. Sugimoto, *J. Am. Ceram. Soc.* **82**(2), 269–279 (1999)
2. H. Zhao, X. Sun, C. Mao, D. Jun, *Phys. B* **404**, 69–72 (2009)
3. K. Kamala Bharathi, J. Arout Chelvane, G. Markandeyulu, *J. Magn. Magn. Mater.* **321**, 3677–3680 (2009)
4. K.K. Bharathi, K. Balamurugan, P.N. Santhosh, M. Pattabiraman, G. Markandeyulu, *Phys. Rev. B* **77**(1–4), 172401 (2008)
5. C.W. Nan, M.I. Bichurin, S. Dong, D. Viehland, G. Srinivasan, *J. Appl. Phys.* **103**(031101), 1–35 (2008)
6. M.M. Rashada, E.M. Elsayeda, M.M. Moharama, R.M. Abou-Shahbab, A.E. Saba, *J. Alloys Compd.* **486**, 759–767 (2009)
7. M. Mozaffari, Z. Aboalizadeh, J. Amighian, *J. Magn. Magn. Mater.* **323**, 2997–3000 (2011)
8. S.E. Shirsath, S.S. Jadhav, B.G. Toksha, S.M. Patange, K.M. Jadhav, *J. Appl. Phys.* **110**(013914), 1–8 (2011)
9. J.H. Nam, W.K. Kim, S.J. Park, *Phys. Stat. Sol.* **201**(8), 1838–1841 (2004)
10. S.J. Yuan, K. Xu, L.M. Yu, S.X. Cao, J.C. Zhang, *J. Magn. Magn. Mater.* **314**, 100–104 (2007)
11. L.G. Van Uitert, *J. Chem. Phys.* **24**, 306–310 (1956)
12. Y. Shi, J. Ding, *J. Appl. Phys.* **90**, 4078–4084 (2001)
13. R.N. Bhowmik, *Mater. Res. Bull.* **50**, 476–482 (2014)
14. F.F. Fava, I. Baraille, A. Lichanot, C. Larrieu, R. Dovesi, *J. Phys. Condens. Matter* **9**, 10715–10724 (1997)
15. S. Tsunekawa, K. Ishikawa, Z.Q. Li, Y. Kawazoe, A. Kasuya, *Phys. Rev. Lett.* **85**, 3440–3443 (2000)
16. P.P. Chatterjee, S.K. Pabi, I. Manna, *J. Appl. Phys.* **86**, 5912–5914 (1999)
17. R. Banerjee, E.A. Sperling, G.B. Thompson, H.L. Fraser, S. Bose, P. Ayyub, *Appl. Phys. Lett.* **82**, 4250–4252 (2003)
18. L. Wang, F.S. Li, *J. Magn. Magn. Mater.* **223**, 233–237 (2001)
19. K.S. Aneesh Kumar, R.N. Bhowmik, *Mater. Chem. Phys.* (2014) <http://dx.doi.org/10.1016/j.matchemphys.2014.03.015>
20. J. Azadmanjiri, S.A. Seyyed Ebrahimi, *Phys. Stat. Sol.* **1**(12), 3414–3417 (2004)
21. S. Verma, P.A. Joy, *Mater. Res. Bull.* **43**, 3447–3456 (2008)
22. D.T.T. Nguyeta, N.P. Duonga, L.T. Hunga, T.D. Hiena, T. Satoh, *J. Alloys. Compd.* **509**, 6621–6625 (2011)
23. X. Cao, H. Dong, J. Meng, J. Sun, *Solid State Sci.* **13**, 1804–1808 (2011)
24. R. Zboril, M. Mashlan, K. Barcova, M. Vujtek, *Hyperfine Interact.* **139**(140), 597–606 (2002)
25. D.E. Zhang, X.J. Zhang, X.M. Ni, H.G. Zheng, D.D. Yang, *J. Magn. Magn. Mater.* **292**, 79–82 (2005)
26. J. Jacob, M. Abdul Khadar, *J. Appl. Phys.* **107**(114310), 1–10 (2010)
27. P.R. Graves, C. Johnson, J.J. Campaniello, *Mater. Res. Bull.* **23**, 1651–1660 (1988)
28. A. Ahlawat, V.G. Sathen, V.R. Reddy, A. Gupta, *J. Magn. Magn. Mater.* **323**, 2049–2054 (2011)
29. J.A.C. de Paiva, M.P.F. Graca, J. Monteiro, M.A. Macedo, M.A. Valente, *J. Alloys, Compd.* **485**, 637–641 (2009)
30. C. Baratto, P.P. Lottici, D. Bersani, G. Antonioli, *J. Sol-Gel. Sci. Technol.* **13**, 667–671 (1998)
31. W. Wang, Y. Liu, C. Xu, C. Zheng, G. Wang, *Chem. Phys. Lett.* **362**, 119–122 (2002)
32. M.W. Kadi, R.M. Mohamed, *Ceram. Inter.* **40**, 227–232 (2014)
33. R. Topkaya, O. Akman, S. Kazan, B. Aktas, Z. Durmus, A. Baykal, *J. Nanopart. Res.* **14**(1156), 1–16 (2012)
34. K.K. Bharathi, R.J. Tackett, C.E. Botez, C.V. Ramana, *J. Appl. Phys.* **109**(1–3), 07A510 (2011)
35. B. Ghosh, M. Sardar, S. Banerjee, *J. Appl. Phys.* **114**(183903), 1–4 (2013)
36. C. Klewe, M. Meinert, A. Boehnke, K. Kuepper, E. Arenholz, A. Gupta, J.-M. Schmalhorst, T. Kuschel, G. Reiss, *J. Appl. Phys.* **115**(123903), 1–6 (2014)
37. B.D. Cullity, C.D. Graham, *Introduction to Magnetic Materials*, 2nd edn. (John Wiley & Sons, Inc., Hoboken, New Jersey, 2009)
38. G.C.P. Leite, E.F. Chagas, R. Pereira, R.J. Prado, A.J. Terezo, M. Alzamora, E. Baggio-Saitovitch, *J. Magn. Magn. Mater.* **324**, 2711–2716 (2012)
39. M.F. Hansen, S. Morup, *J. Magn. Magn. Mater.* **203**, 214–216 (1999)
40. D. Kechrakos, K.N. Trohidou, *J. Magn. Magn. Mater.* **262**, 107–110 (2003)
41. S. Chandra, H. Khurshid, W. Li, G.C. Hadjipanayis, M.H. Phan, H. Srikanth, *Phys. Rev. Lett.* **86**(014426), 1–8 (2012)
42. J.H. He, S.L. Yuan, Y.S. Yin, Z.M. Tian, P. Li, Y.Q. Wang, K.L. Liu, C.H. Wang, *J. Appl. Phys.* **103**(023906), 1–4 (2008)

43. V. Sepelak, D. Baabe, D. Mienert, D. Schultze, F. Krumeich, F.J. Litterst, K.D. Becker, J. Magn. Magn. Mater. **257**, 377–386 (2003)
44. M.A. Dar, J. Shah, W.A. Siddiqui, R.K. Kotnala, J. Alloys Compd. **523**, 36–42 (2012)
45. M.P. Proenca, C.T. Sousa, A.M. Pereira, P.B. Tavares, J. Ventura, M. Vazquez, J.P. Araujo, Phys. Chem. Chem. Phys. **13**, 9561–9567 (2011)
46. R.V. Morris, H.V. Lauer Jr, C.A. Lawson, E.K. Gibson Jr, G.A. Nace, C. Stewart, J. Geophys. Res. **90**(B4), 3126–3144 (1985)